Maria DEMS, Krzysztof KOMĘZA

Technical University of Lodz, Institute of Mechatronics and Information Systems

Determination of parameters of a high-speed induction motor using the field-circuit and analytical method

Abstract. *The paper presents the field-circuit and circuit modelling of the no-load and load losses in the core of high-speed induction motor. The machine parameters and load characteristics are calculated at supply frequencies of 50, 100 and 200 Hz. In the field-circuit approach the distribution and changes of magnetic flux density in the motor are computed using a time-stepping finite element method. The Discrete Fourier Transform is used to analyze the magnetic flux density waveforms in each element of the motor model. The influence of load condition on core losses has been observed. The results are compared with measurements.*

Streszczenie. *W artykule przedstawiono modelowanie obwodowo-polowe i obwodowe strat w rdzeniu wysokoobrotowego silnika indukcyjnego w stanie jałowym i podczas obciążenia. Parametry i charakterystyki obciążeniowe zostały obliczone przy częstotliwości napięcia zasilającego 50, 100 i 200 Hz. Rozkład pola magnetycznego w silniku obliczono z wykorzystaniem time-stepping metody elementów skończonych. Do analizy strumienia magnetycznego w każdym elemencie modelu silnika wykorzystano dyskretna transformatę Fouriera. Pokazano wpływ obciążenia na straty w rdzeniu silnika. Wyniki obliczeń porównano z wynikami pomiarów. (**Modelowanie strat w rdzeniu wysokoobrotowego silnika indukcyjnego w stanie jałowym i podczas obciążenia**).*

Keywords: induction motors, core losses, finite element method, circuit modelling.
Słowa kluczowe: silnik indukcyjny, straty w rdzeniu, metoda elementów skończonych, modelowanie obwodowe

Introduction

Core losses generated in small size high-speed induction motors constitute a significant part of total losses in the motor, in particular at higher frequencies. Precise determination of these losses is vital to assure the proper functioning of the motor. Core losses in electrical machines depend on the power loss density of the electrical sheets used, which in turn depends strongly on frequency, magnitude and form of the applied magnetic field [1,5-11]. The specific losses are usually only given for the 50 Hz alternating flux. Consequently, various estimations are applied for higher frequencies. To avoid errors associated with such an approach a direct use of specific losses measured on ring samples has been proposed. The no-load and load losses in the core have been calculated using a field-circuit and a circuit method. The machine parameters and load characteristics have also been determined at supply frequencies of 50, 100 and 200 Hz. The computational results have been verified against measurements.

Object of investigation

The small four-pole energy-saving induction motors with cores made from non-oriented silicon steel M600-50A have been examined.

The supply voltage is 400 V at frequency 200 Hz, which – at a constant ratio of voltage over frequency – is equivalent to 100 V at 50 Hz. The stator windings are star connected and the number of turns in series is 156. There are 24 stator slots and 22 rotor slots. The motor has rotors with closed slots. The external diameter of the stator core is 120 mm, the internal diameter 70.05 mm, and stator core lengths 102 mm. The thickness of the air gap used in calculations was assumed to be 0.225 mm.

The field-circuit modelling

For the purpose of modelling the performance of the motor the RM module of the commercial software OPERA 2D has been used, which combines a time-stepping finite element method (FEM) with a circuit description of the windings to account for the resistances and inductances of the end connections. The resistances and inductances of the sections of rotor bars extending beyond the laminations, and those of end rings, have also been modelled as external circuits. To calculate the relevant inductances classical analytical equations have been applied as used in equivalent circuits formulations and verified using 3D finite element modelling. As a result the following differential equations have been formed:

$$(1)\quad \begin{bmatrix} \mathbf{G} & \mathbf{H} & \mathbf{0} \\ \mathbf{0} & \mathbf{W} & \mathbf{D} \\ \mathbf{0} & \mathbf{D}^{\mathbf{T}} & \mathbf{R} \end{bmatrix} \begin{bmatrix} \mathbf{A} \\ \mathbf{\Delta V} \\ \mathbf{i} \end{bmatrix} + \begin{bmatrix} \mathbf{Q} & \mathbf{0} & \mathbf{0} \\ \mathbf{H}^{\mathbf{T}} & \mathbf{0} & \mathbf{0} \\ \mathbf{0} & \mathbf{0} & \mathbf{L} \end{bmatrix} \frac{\partial}{\partial t} \begin{bmatrix} \mathbf{A} \\ \mathbf{\Delta V} \\ \mathbf{i} \end{bmatrix} = \begin{bmatrix} \mathbf{J} \\ \mathbf{0} \\ \mathbf{U} \end{bmatrix}$$

where:

$$G_{ij} = \int \frac{1}{\mu} \Delta N_i \Delta N_j dS \qquad H_{ij} = \int_k \gamma N_i dS$$

$$W_{kk} = \int_k \gamma dS \qquad Q_{ij} = \int \gamma N_i N_j dS \qquad J_i = \int J_0 N_i dS$$

and **D** is an 'index matrix', with elements +1 or −1, indicating the position of the bar in the circuit.

At both the light-running and load tests the rotor revolved with constant speed. To allow for such movement special 'air-gap' elements were used, with similarly sized 'normal' elements on either side, to connect the stationary stator and moving rotor. As the gap is very small (0.225 mm) the usual subdivision into three layers has not been applied. There are 528 air-gap elements around the circumference of the gap and altogether 41872 elements of the finite element mesh. The number and size of the elements has a direct effect on the accuracy of the computation.

The core losses are calculated from the time variation of the module of flux density components in all elements. As first-order elements have been used, the flux density is constant in each element; thus the mesh resolution (density) is crucial for the accuracy of computation. The time variation is taken at 100 'snapshots' over one cycle and analysed using the Discrete Fourier Transform (DFT) to calculate harmonics, for which losses are then estimated. These calculations rely on approximated curves of losses for lamination sheets at given frequency measured on a ring sample. The results of loss calculations for light-running and load conditions at 50 Hz suggest that accounting for the movement of the rotor is necessary to achieve good accuracy.

Under load conditions the losses increase significantly compared with the light-running condition. This is primarily due to local magnetic saturation of the rotor teeth tips (the 'bridging' connections between teeth) – as illustrated in Fig. 1 – and the effect of the tooth ripple (slot leakage flux). Figures from 2 to 5 show the flux distributions for selected harmonics under light-running and load conditions for frequency 50 Hz.

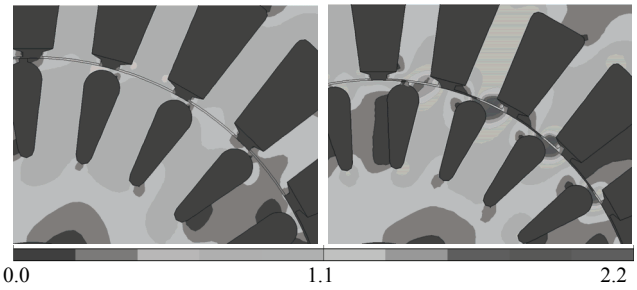

Fig.1. Comparison of the flux density distributions in the gap region under load (right) and at no load (left).

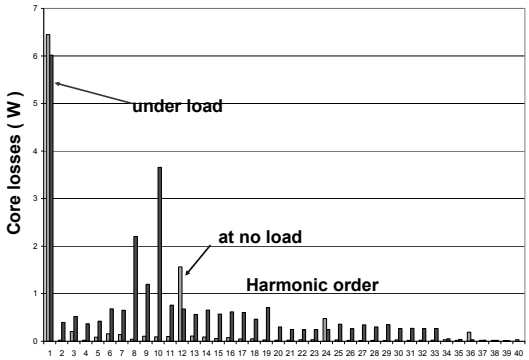

Fig.2. Comparison of core loss spectrum calculated at no load and under load for 50 Hz.

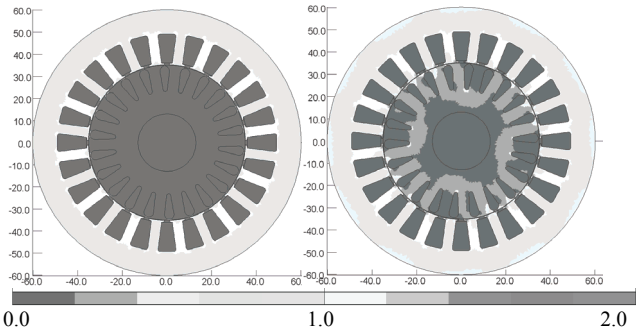

Fig.3. Comparison of the flux density distributions for the 1th harmonic at no load and under load for 50 Hz.

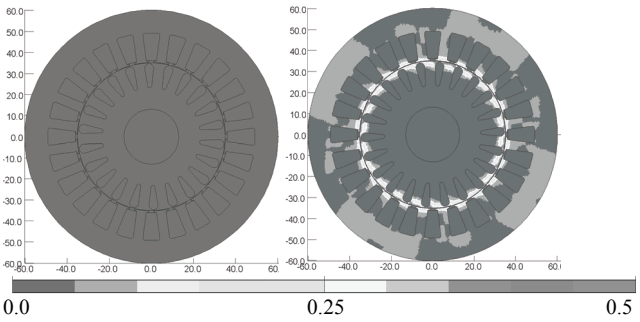

Fig.4. Comparison of the flux density distributions for the 10th harmonic at no load and under load for 50 Hz.

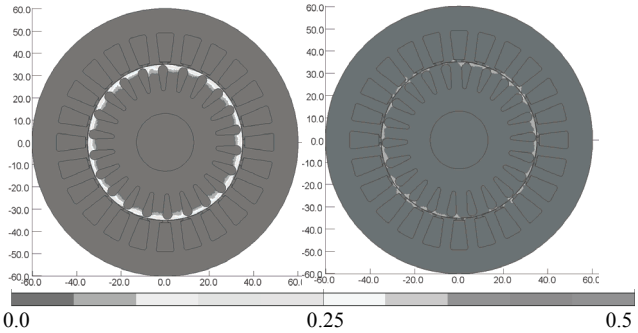

Fig.5. Comparison of the flux density distributions for the 10th harmonic at no load and under load for 50 Hz.

Figure 6 shows the spectrum of core losses under light-running and load conditions for 100 Hz. Figures from 7 to 9 present the flux distributions for selected harmonics under light-running and load conditions for frequency 100 Hz

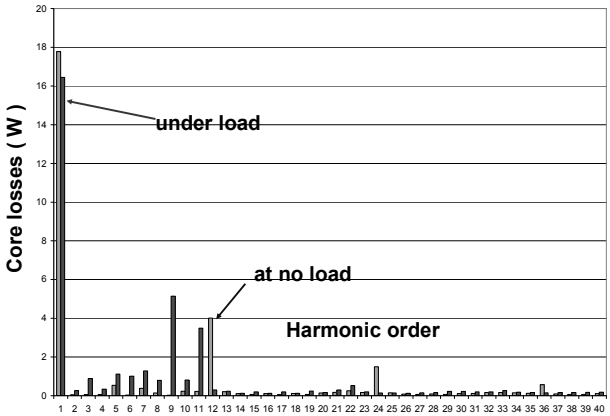

Fig.6. Comparison of core loss spectrum calculated at no load and under load for 100 Hz.

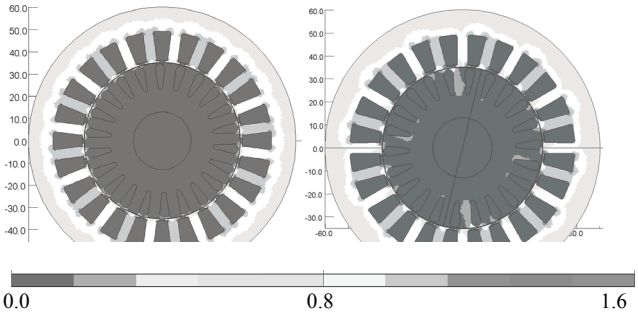

Fig.7. Comparison of the flux density distributions for the 1th harmonic at no load and under load for 100 Hz.

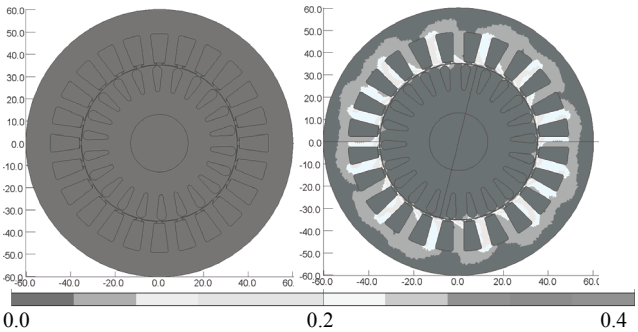

Fig.8. Comparison of the flux density distributions for the 9th harmonic at no load and under load for 100 Hz.

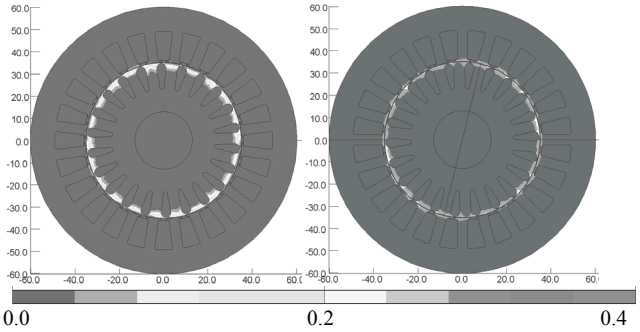

Fig.9. Comparison of the flux density distributions for the 12th harmonic at no load and under load for 100 Hz.

Under load the iron losses are over three times bigger than under no load. This results from the disappearance of the positive effect of the closing of the teeth tips (observed under no load) due to the saturation caused by the rotor tooth leakage flux and the effect of the rotation of this flux on the stator surface leading to generation of losses in the surface layer of the stator (clearly visible for example for the 8th harmonic). The losses due to the 1st harmonic are practically the same under the two conditions, while new harmonics occur when load is applied generating these additional losses not present at no load.

The circuit calculations

In core loss calculations based on an equivalent circuit model of the core only the first harmonic of the field was taken into account [3]. The results of the no-load core loss calculations were presented in [2, 4]. The higher harmonics of the magnetic field in the air-gap were then considered in the calculation of the additional no-load core loss.

Under the load conditions, the additional surface loss $P_{s\nu}$ in the stator and rotor teeth, caused by the flux of the $\nu_{r(s)}$ order harmonic rotor and stator fields and additional pulsation losses in the stator teeth $P_{p\nu}$, caused by the flux of the harmonic rotor fields, were calculated using similar expressions as used for the no load condition reported in [12], taking the relevant flux density harmonic under particular load conditions.

In the calculations of the total losses of the motor the following were taken into account:

- additional pulsation losses in the rotor cage, caused by the flux of the harmonic stator field,
- additional losses caused by the skew of rotor slots,
- additional losses in the end winding of the motor,
- saturation of magnetic core of the motor,
- skin-effect in the rotor bar.

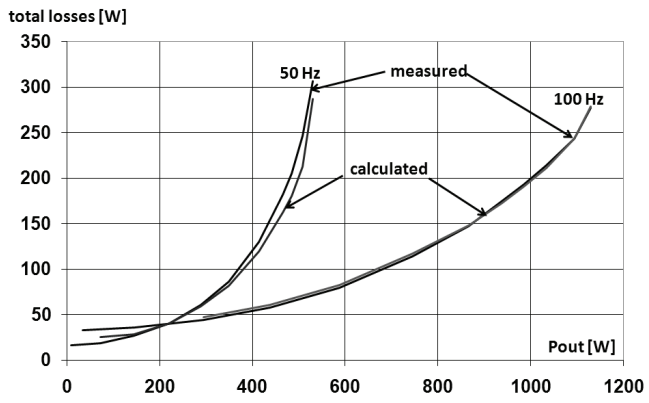

Fig.10. Total losses versus output power of the motor calculated using the circuit model and measured.

Figure 10 shows the total losses versus mechanical power P_{out}, measured and calculated with the use of the circuit model, for different values of the frequency [14].
Figures 11 - 12 present the performance characteristics of the motor versus mechanical power P_{out}, measured and calculated with the use of the circuit model.

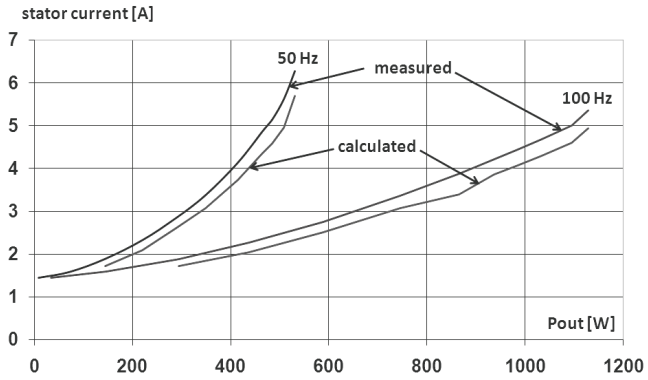

Fig.11. Stator current versus output power of the motor calculated using the circuit method and measured

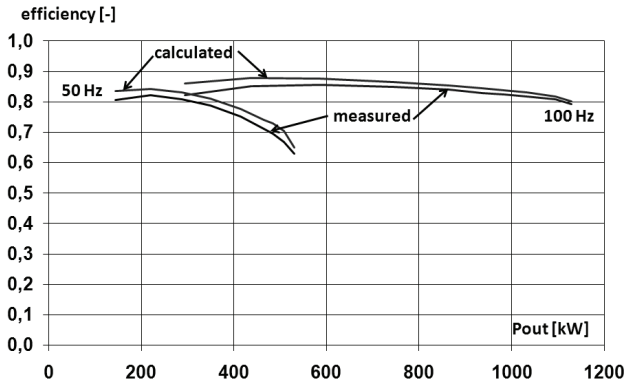

Fig.12. Efficiency versus output power of the motor calculated using the circuit method and measured.

Figures 13 and 14 show the current and torque versus speed (slip) characteristics, calculated and measured, at two frequencies. At 50 Hz the results are given for different temperatures of the stator and the rotor, as during the tests the temperature changed. As can be seen the calculated values are between the bounds provided by different temperatures.

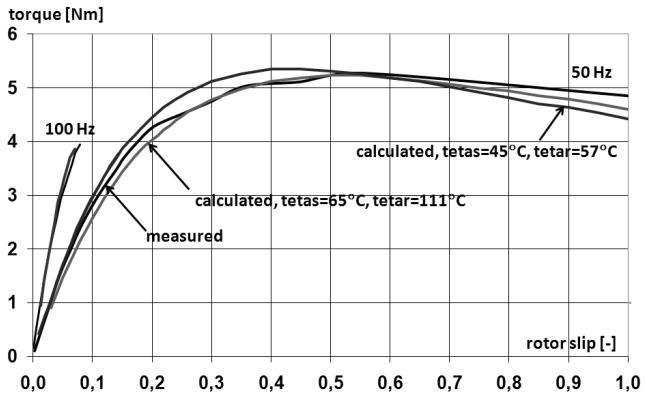

Fig.13. Torque/slip curve, calculated using the circuit method and measured.

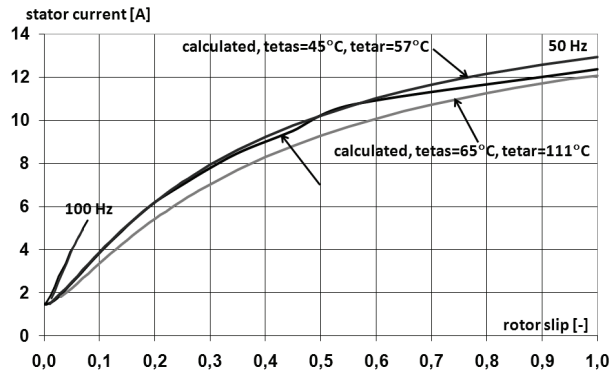

Fig.14. Stator current versus slip curve, calculated using the circuit method and measured.

Final results

Selected performance parameters calculated at frequencies 50 and 100 Hz are presented in Table I and compared with measurements.

Table 1. Basic and additional no-load core losses calculated using the field-circuit and circuit model and measured

	50 Hz		100 Hz	
	Calculated using field-circuit method	Calculated using circuit method	Calculated using field-circuit method	Calculated using circuit method
Stator current [A]	5.65	5.69	4.51	4.94
measured	6.27		5.37	
Input electrical power [W]	813	817	1341.3	1408
measured	843		1424	
Short-circuit current [A]	12.62	12.51	20.915	--
measured	12.37		--	
Short-circuit torque [Nm]	4.42	4.51	7.79	--
measured	4.83		--	
Load core losses [W]	31.67	32.91	78,23	85.36

Minor discrepancies between measurements and simulation may be attributed to changes in magnetic properties of the laminations occurring during the technological processes. The rotor and stator laminations are punched together.

The rotor sheets are then assembled and aluminium is cast. Finally, the rotor is machined to achieve the desired thickness of the air-gap. All these manufacturing stages affect the magnetic properties, in particular in areas close to the air-gap; such changes are very difficult to quantify. It is noted that the calculated active component of the stator current is in good agreement with experiment, whereas the magnetizing component is below the measured value – this suggests the above to be the most likely explanation.

Figure 15 show the total losses of the motor measured and calculated versus mechanical power P_{out} with the use of the circuit model for frequency 200 Hz. The measurement results were obtained for inverter supply with rms voltage value of 436 V. Due to the fact that the circuit model is mono-harmonic, calculations were made assuming the motor is supply by an alternating sinusoidal voltage of rms value 400 V. Figure 16 compare the values of calculated and measured stator current. One can observe that measured values of stator current are slightly bigger then measured. The main reason for this phenomenon is disregarded in the circuit calculation higher harmonic of stator current. Calculated total losses curve crosses the measured curve. Since for the whole range measured current is bigger than calculated the reason for this occurrence must be core losses. The calculated core losses are growing faster than the measured. Despite these differences efficiency characteristics are very similar.

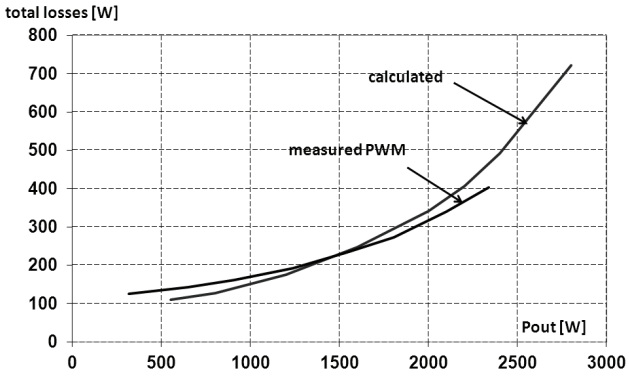

Fig.15. Total losses versus output power of the motor calculated using the circuit model and measured for frequency 200 Hz

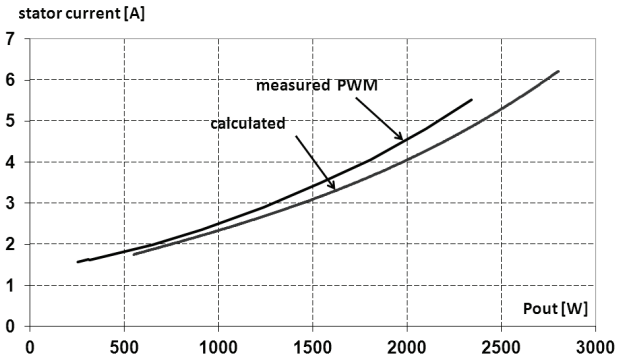

Fig.16. Stator current versus output power of the motor calculated using the circuit method and measured for frequency 200 Hz

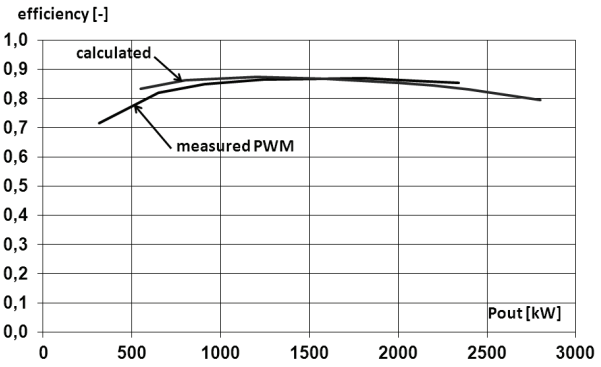

Fig.17. Efficiency versus output power of the motor calculated using the circuit method and measured. for frequency 200 Hz

Figures 18 and 19 show the current and torque versus speed (slip) characteristics, calculated and measured, at frequency 200 Hz. Based on the comparison of measured and calculated curves can be stated that the use of mono-harmonic circuit model for the motor supply by PWM inverter is fully acceptable.

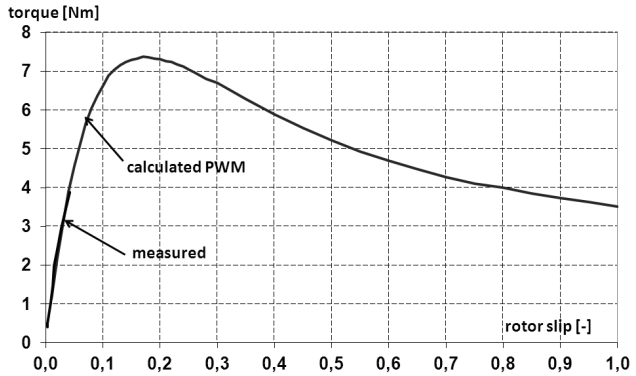

Fig.18. Torque/slip curve, calculated using the circuit method and measured for frequency 200 Hz

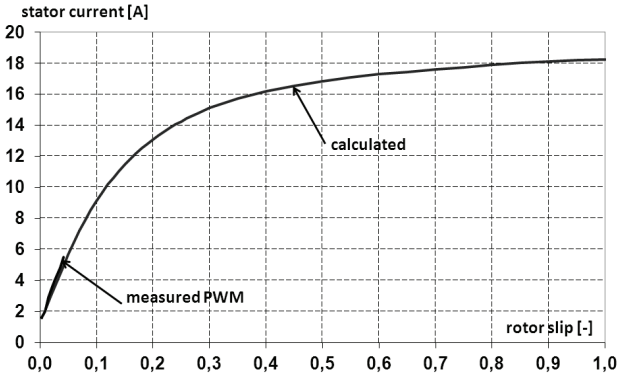

Fig.19. Stator current versus slip curve, calculated using the circuit method and measured for frequency 200 Hz.

The accuracy of the simulation mainly depends on the shape of the supply voltage. The lower order harmonics with significant amplitude cause additional core losses and disturbances in stator current shape versus time.

Conclusion

The paper describes a method to calculate performance characteristics and core losses of a high speed induction motor supplied at 50 and 100 Hz. The results of the field-circuit and circuit formulations used are in good agreement with measurements. A significant increase of the core losses has been observed between the light-running and full-load conditions. The comparison between calculated, using circuit approach and supply by fundamental harmonic of the phase voltage, and measured characteristics of the motor shows that the results achieved are satisfactory.

Acknowledgments: The authors gratefully acknowledge the contributions of J. Szulakowski from TU Lodz for his work on core losses measurements and of A. Michaelides from Vector Fields Software Cobham Technical Services for valuable help.

This work was supported by the Ministry of Science and Higher Education (Project N N510 388235).

REFERENCES

[1] D. Ionel, M. Popescu, C. Cossar, M.I. McGilp, A. Boglietti, A. Cavagnino, "A General Model of the Laminated Steel Losses in Electric Motors with PWM Voltage Supply", in I*ndustry Applications Society Annual Meeting 2008*, pp. 1-7.

[2] M. Dems M., K. Komęza, J Szulakowski., "No-Load Curves of the High-Speed Small Size Induction Motor", *ZP-ME*, vol. 82, pp. 239-245 Katowice, Poland, 2009,

[3] Komęza K., Dems M., Szulakowski J.: Advanced Computer Modelling of no-load curves of the high-speed small size induction motors, Electrical Review, R.86 Nr 5/2010, pp. 152-155.

[4] A. Tessarolo, F. Luise, "A finite element approach to harmonic core loss prediction in VSI-fed induction motor drives" in International Symposium on Power Electronics, Electrical Drives, Automation and Motion SPEEDAM 2008, pp. 1309 – 1314.

[5] E. Dlala, A. Belahcen, J. Pippuri, A. Arkkio, "Interdependence of Hysteresis and Eddy-Current Losses in Laminated Magnetic Cores of Electrical Machines", *IEEE Trans. on Mag.*, Vol. 46 , Issue 2,pp. 306 – 309, 2010.

[6] E. Dlala, "Comparison of Models for Estimating Magnetic Core Losses in Electrical Machines Using the Finite-Element Method", IEEE Trans. on Mag., vol. 45, issue 2, part 1, pp. 716 – 725, Feb. 2009.

[7] A. Belahcen, A. Arkkio, "Comprehensive Dynamic Loss Model of Electrical Steel Applied to FE Simulation of Electrical Machines", *IEEE Trans. on Mag.,* Vol.44 , Issue 6, pp. 886 - 889, 2008.

[8] S.O.Kwon, J.J. Lee, B.H. Lee, J.H. Kim, K.H. Ha, J.P. Hong, "Loss Distribution of Three-Phase Induction Motor and BLDC Motor According to Core Materials and Operating", *IEEE Trans. on Mag.,* Vol. 45 , Issue 10, pp. 4740 – 4743, 2009.

[9] J. G. Zhu, V. S. Ramsden, "Improved formulations for rotational core losses in rotating electrical machines", *IEEE Trans. Magn.*, 34, pp. 2234–2242, 1998.

[10] L. Yujing, S. K. Kashif, A. M. Sohail, "Engineering considerations on additional iron losses", *Proc. 18th International Conference on Electrical Machines ICEM 2008*, pp. 1-4.

[11] T. Śliwiński, "The methods of the induction motors calculation", *PWN*, Warszawa, Poland, 2008, p.324 (in polish)

[12] Piepenbreier B., Taegen F., "Surface losses in cage induction motors" in *Proc. Beijing International Conference on Electrical Machines*, China Academic Publishers, Book I, pp. 326-329, 1987.

[13] Dems M., Rutkowski Z., Computer program STAT_WIN_F v.2 "Electromagnetical calculation of high-speed induction motor" *Computer programs library of Institute of Mechatronics and Information Systems, Technical University of Lodz*, Poland, 2010

***Authors**: dr hab. inż. Maria Dems, prof. PŁ, dr hab. inż. Krzysztof Komęza, prof. PŁ, Technical University of Lodz, Institute of Mechatronics and Information Systems, ul. Stefanowskiego 18/22 90-924 Lodz, Poland, e-mail: maria.dems@p.lodz.pl krzysztof.komeza@p.lodz.pl*